Dynamic features of cardiac vector as alternative markers of drug-induced spatial dispersion

Pablo Daniel Cruces [a,b] Drago Torkar [c] Pedro David Arini [a,b]

[a] *Instituto de Ingeniería Biomédica, UBA, Paseo Colón 850 (C1063ACV), Buenos Aires, Argentina*
[b] *Instituto Argentino de Matemática 'Alberto P. Calderón', CONICET, Saavedra 15 (C1083ACA), Buenos Aires, Argentina*
[c] *Institut 'Jožef Stefan', Department of Computer Systems, Jamova cesta 39 (SI-1000), Ljubljana, Slovenia*

Corresponding Author at: Pablo Daniel Cruces, Saavedra 15, CABA (C1083ACA), Argentina; pcruces@fi.uba.ar; 0054-11-4954-6781 int 121.

Preprint submitted to *May 24, 2020*

Abstract

Introduction: The abnormal amplification of ventricular repolarization dispersion (VRD) has long been linked to proarrhythmia risk. Recently, the measure of VRD through electrocardiogram intervals has been strongly questioned. The search for an efficient and non-invasive surrogate marker of drug-induced dispersion effects constitute an urgent research challenge. **Methods:** Herein, drug-induced ventricular dispersion is generated by d-Sotalol supply in an In-vitro rabbit heart model. A cilindrical chamber simulates the thorax and a multi-electrode net is used to obtain spatial electrocardiographic signals. Cardiac vector dynamics is captured by novel velocity cardiomarkers obtained by quaternion methods. Through statistical analysis and machine learning technics, we compute potential dispersion markers that could define proarrhythmic risk. **Results:** The cardiomarkers with the greatest statistical significance, both obtained from the electrical cardiac vector, were: the QT_ω, which is the difference between first and last maxima of angular velocity and $\lambda 21_v^T$, the roundness of linear velocity. When comparing with the performance of the current standards (89%), this pair was able to correctly separate 21 out of 22 experiments achieving a performance of 95%. Moreover, the QT_ω computes in a much more robust basis the QT interval, the current index for drug regulation. **Discussion:** These velocity markers circumvent the problems of accuratelly finding the fiducial points such as the always tricky T-wave end. Given the high performance they achieved, it is provided a promising outcome for future applications to the detection of anomalous changes of heterogeneity that may be useful for the purposes of torsadogenic toxicity studies.

Keywords

Cardiac electrical vector, Heterogeneity, Proarrhythmic side effects, Quaternion methods, Sotalol.

1. Introduction

In most medications with proarrhythmic side effects, the inhibition of the rapid component of the delayed rectifier potassium current (I_{Kr}) induce a spatial amplification of ventricular repolarization dispersion (VRD). This fact is usually observed as a prolongation of QT interval (current international drug regulation ICH S7B/E14 [1,2]) which is a non-invasive electrocardiographic measure of total time of ventricular depolarization and repolarization. Moreover, this phenomenon has also been observed in several markers of VRD such as the T_{PE} and the JTp, associated with trasmural and apico-basal dispersion respectively [3]. On the other hand, many other drugs affect multiple ion channels during cardiac repolarization and they also prolong QT interval. In fact, beyond the key factor of the delay in repolarization due to I_{Kr} blockage, it is required the activation of inward late sodium or calcium currents to trigger a proarrhythmic response [4].

The abnormal amplification of VRD has long been recognised as a key factor to underlying arrhythmogenic mechanisms responsible for severe arrhythmias [5]. Recently, the measure of VRD through electrocardiogram (ECG) intervals has been strongly questioned [6,7]. Additionally, although QTc regulation prevented the release of drugs with proarrhythmic substrates, it also discouraged the development of other beneficial and safe medicines as a consequence of the large number of false positives of the method [8]. It is the same with similar surrogate markers T_{PE} and JTp where, unfortunately, the specificity is still inadequate probably as a result of the uncertainty in the delineation of the end of the ventricular repolarization. In this regard, the U.S. Food and Drug Administration has highlighted the need to complement current studies with more sensitive indices of dispersion for optimization of therapeutic strategies [9].

Currently, many multidisciplinary teams of scientists are working to develop novel VRD markers in order to achieve an effective prediction of clinical proarrhythmia risk [10,11]. With the aim of offering a contribution to this major problem, we evaluate novel velocity cardiomarkers obtained through quaternionic methods using an In-vitro heart model. Herein, ventricular heterogeneity is generated by d-Sotalol supply. Sotalol is a beta-blocker agent with Class III antiarrhythmic activity, currently used in atrial fibrillation treatment. It increases the spatial VRD via non-uniform I_{Kr} inhibition and it has long been reported its high incidence of Torsade de Pointes. According to a recent study in intact human hearts, differences in upslopes of T-wave reflect intra-cardiac repolarization dispersion [12]. We have previously shown that T-wave slopes are related to cardiac vector velocities, which have been greatly useful in the diagnosis of myocardial infarction [13] and in the detection and localization of acute myocardial ischemia [14]. Also, it has been reported the relevance of the conduction velocity and the nouniformity of the excitability of the myocardial action potentials in the induction of malignant arrhythmias [15]. We propose then that the velocity cardiomarkers, obtained from non-invasive vectorcardiograms, could reflect the amplification of VRD more efficiently than classical ECG intervals. Additionally, since the current markers are affected by the problem of the detection of the onset and end of the T-waves, we also report an alternative way to measure QT interval from angular velocity computation during depolarization and repolarization.

2. Materials and methods

2.1. *Isolated rabbit heart database*

All the recordings used in this work have been acquired from N=11 New Zelland white rabbits. All of them were male and weight ranged from 2.8 to 3.8 kg. Briefly, the rabbits were anesthetized (35 mg/kg Ketamine and 5 mg/kg Xylocaine) following heparinization (500 U/kg IV), intramuscular injection in both cases. The chest was opened and the heart was removed and arrested by immersion in ice-cold Tyrode solution. Then, it was mounted in a Langendorff apparatus and was retrogradely perfused through the aorta with Tyrode's solution (in mM - $140\ NaCl$, $5\ KCl$, $1\ MgCl_2$, $0.33\ NaH_2PO_4$, $5\ HEPES$, $11.1\ glucose$, $2\ CaCl_2$). The perfusate heated up to $38°C\ \pm\ 0.5°C$ and continuously gassed with 100% O_2. Pressure was maintained at 70 mmHg and pH was set to 7.4. Right atrium was paced at 2Hz following crashing of sinus node.

The heart was immersed in a cylindrical chamber, which simulates the rabbit thorax, with an array of parallel and equally spaced leads (see Fig. 1a). Two signals were acquired: 1) Control recording was made after 30 minutes period of cardiac equilibration; 2) d-Sotalol recording ($60\mu M$) again measured after 30 minutes of drug perfusion. Each signal was digitized with the sampling frequency (**Fs**) of 500 samples per second and 12 bit resolution. The drug concentration was chosen based on the usual range in In-vitro rabbit heart studies [16,17]. These studies usually covers a large range: $1\mu M$ to $500\mu M$, in comparison with the therapeutic range of concentration used in humans $4\mu M$ to $37\mu M$ [18,19,20]. The aim of our model was to define dispersion quantifiers since its increase has been associated with the risk of arrhythmias. For this reason, the concentration used it is high enough to generate cardiac dispersion and at the same time, the range of values with high incidence of Torsade de Pointes in the isolated heart has been avoided (over values greater than $100\mu M$) [21].

This database has been previously published in [22]. This study was approved by Clinical and Research Bioethics Committee and animals were cared for according to Argentinian National Drugs, Food and Medical Technology Administration Standards (Regulation 6344/96) and the US National Institutes of Health guide for the care and use of laboratory animals (NIH publication number 85-23, revised 1996).

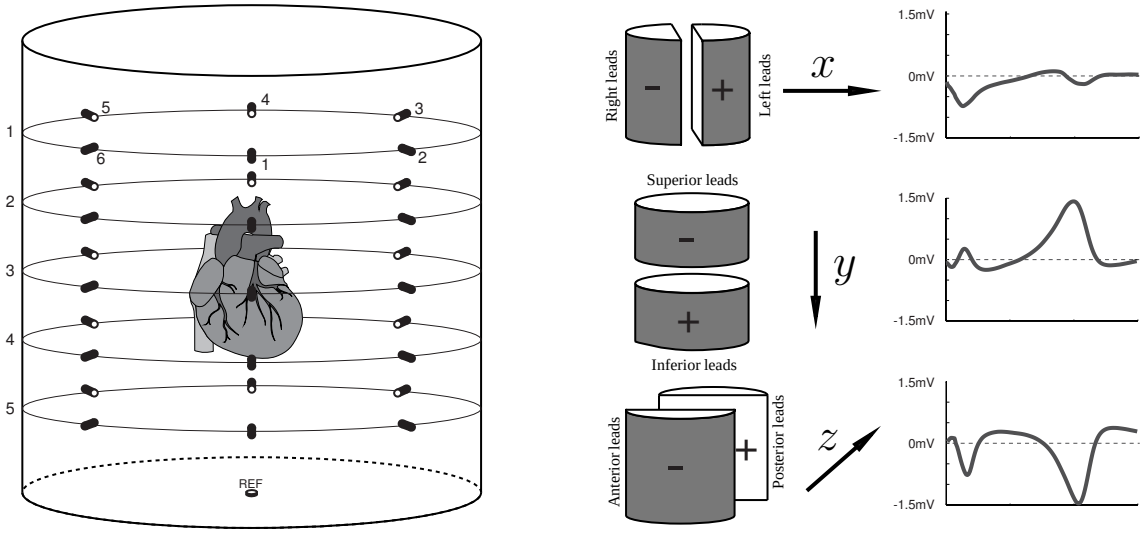

(a) Heart chamber and its electrode matrix

(b) XYZ signals derivation from the 30-leads matrix

Figure 1. (a) Diagram of experimental setup which simulates the rabbit thorax. The chamber is 10cm high x 10cm in diameter. The 30-electrodes are Ag-AgCl of 2mm in diameter. The leads (L) array is ordered in a 5 x 6 matrix according the numbering shown; (b) Computation of spatial information. Differences between right and left leads constitute the projection of the electrical activity on x-axis. Inferior-superior and posterior-anterior leads define the same for y-axis and z-axis respectively.

2.2. *3D-Spatial representation*

In order to evaluate how drug-induced ventricular dispersion is reflected in the cardiac vector dynamics, a three-dimensional representation is built. As shown in Fig. 1b, from the information collected by the 30-electrodes array (so-called L matrix), the projection of the electrical activity on each coordinate axis can be reconstructed from the following expressions:

– The differences between the right and the left leads constitute the projection of the electrical activity on x-axis. This projection is obtained as:

$$\mathbf{x} = \frac{\sum_{i=1}^{5} \left(\sum_{j=(2,3)} L_{ij} - \sum_{j=(5,6)} L_{ij} \right)}{20} \tag{1}$$

– The projection of the electrical activity on y-axis was computed as the differences between inferior and superior leads, as follows:

$$\mathbf{y} = \frac{\sum_{j=1}^{6} \left(\sum_{i=(4,5)} L_{ij} - \sum_{i=(1,2)} L_{ij} \right)}{24} \tag{2}$$

– Finally, the differences between posterior and anterior leads constitute the projection of the electrical activity on z-axis, calculated as:

$$\mathbf{z} = \frac{\sum_{i=1}^{5} \left(\sum_{j=(3,4,5)} L_{ij} - \sum_{j=(6,1,2)} L_{ij} \right)}{30} \tag{3}$$

where i refers to rows and j to columns of the 5x6 L-matrix, ie: the 30-electrodes array (see Fig.1b). It should be noted, that given the uniform distribution of electrodes, the normal vector projections to each axis compensate each other.

2.3. *Dynamic features*

The three-dimensional movement of the tip of cardiac vector, obtained from XYZ signals of the representation shown in Eqs. 1, 2 and 3, can be described through the radius and the linear and angular velocities. The **radius** is merely the 2-norm of XYZ vectors, ie given a nth sample point $\mathbf{P_n}(x, y, z)$ of a beat, its radius is defined by $\|\mathbf{P_n}\|_2$. On the other hand, while **linear velocity** can be computed by direct differenciation of the prior vectors (Eq. 4), the angular velocity is quite hard to be computed.

$$\overrightarrow{v_n} = (P_n(\mathbf{x}, \mathbf{y}, \mathbf{z}) - P_{n+1}(\mathbf{x}, \mathbf{y}, \mathbf{z})) \cdot Fs \tag{4}$$

We have previously shown that by means of a quaternion transformation of 3D-space it is possible to obtain the expression of the instantaneous **angular velocity** of the cardiac electrical vector [14]. Quaternions are hypercomplex numbers that constitute a non-commutative field. They are very useful in the study of rotations and it has been shown that they are very efficient in terms of uncertainty propagation and computing time by comparison with traditional methods such as Euler matrices [23]. Every quaternion (Eq. 5) has a real part (associated with an amount of rotation) and three imaginary parts (associated with the rotation axis $\overrightarrow{N}$) that satisfy the Hamilton rule ($\boldsymbol{i}^2 = \boldsymbol{j}^2 = \boldsymbol{k}^2 = \boldsymbol{ijk} = -1$).

$$\mathbf{q_n} = a_1 + a_2\boldsymbol{i} + a_3\boldsymbol{j} + a_4\boldsymbol{k} \quad , \quad a_{1\ldots4} \in \mathbb{R} \tag{5}$$

Similarly, $\mathbf{q_n}$ can be written in terms of a rotation angle α from a XYZ point $\mathbf{P_n}$ to its consecutive point $\mathbf{P_{n+1}}$:

$$\mathbf{q_n} = cos\left(\frac{\alpha}{2}\right) + \overrightarrow{N}.sin\left(\frac{\alpha}{2}\right) \tag{6}$$

where the normal vector $\overrightarrow{N}$ represents the rotation axis. Both trigonometric functions can easily be obtained from dot and cross products between $\mathbf{P_n}$ and $\mathbf{P_{n+1}}$.

$$\begin{cases} P_n \bullet P_{n+1} = \|P_n\|_2.\|P_{n+1}\|_2.cos(\alpha) \\ P_n \times P_{n+1} = \|P_n\|_2.\|P_{n+1}\|_2.sin(\alpha).\overrightarrow{N} \end{cases} \tag{7}$$

then, we can obtain each quaternion for every n instant:

$$\mathbf{q_n} = (P_n \bullet P_{n+1}; P_n \times P_{n+1}) \tag{8}$$

Thus, if we take every point of XYZ signals, we can obtain a sequence of quaternions and thereby we can compute the instantaneous angular velocity by solving the differential Poisson equation [13]. Quaternion inverse can be expressed in terms of its conjugate and its norm: $\mathbf{q}^{-1} = \overline{\mathbf{q}}/\|\mathbf{q}\|^2$.

$$\dot{\mathbf{q}}_\mathbf{n} = \frac{1}{2}.\overrightarrow{\omega_n}.\mathbf{q_n}^{-1} \quad then \quad \overrightarrow{w_n} = (\mathbf{q_{n+1}} - \mathbf{q_i}) \cdot Fs \cdot \frac{\bar{\mathbf{q}}_\mathbf{n}}{\|\mathbf{q_n}\|} \tag{9}$$

2.3.1. *Dispersion markers*

Several quantifiers of dynamic features obtained from both ventricular depolarization (QRS complex loop) and repolarization (T-wave loop) have been selected as potential dispersion markers. We have computed the areas, roundness and maxima of the radius and of each velocity signal loop. We have also computed the current dispersion markers: QT, T_{PE} and absolute areas in QRS complex and T-wave, in order to make a comparison with state-of-art behchmarks.

Absolute signals (ie. 2-norm) of the radius (E) and both velocity signals can be evaluated in terms of their **areas**. As we show in Eq. 10, they have been computed for both QRS complex and T-wave.

$$\begin{cases} A^l_{\mathrm{E}} = \sum_{\forall n \in l} \|E_n\|_2 \\ A^l_v = \sum_{\forall n \in l} \|v_n\|_2 \\ A^l_\omega = \sum_{\forall n \in l} \|\omega_n\|_2 \end{cases} \tag{10}$$

where l is replaced by Q for QRS complex computation or T for T-wave computation.

On the other hand, after a singular value decomposition of the signals (radius and both velocities), we have computed the **first and second eigenvalues** over the total energy: $\lambda 1ET^l_{\mathrm{E}}$ and $\lambda 2ET^l_{\mathrm{E}}$, $\lambda 1ET^l_v$ and $\lambda 2ET^l_v$, $\lambda 1ET^l_\omega$ and $\lambda 2ET^l_\omega$. We have also determined the **ratio of the first two eigenvalues** for each signal in order to evaluate the changes in the "roundness" of each loop: $\lambda 21^l_{\mathrm{E}}$, $\lambda 21^l_v$ and $\lambda 21^l_\omega$.

In addition, we have calculated the **maxima** of the velocities.

$$\begin{cases} M^l_v = max(\|v_n\|_2) \\ M^l_\omega = max(\|\omega_n\|_2) \end{cases} \tag{11}$$

Here it is worth noting that locations of both the first maximum of the angular velocity in QRS and the last maximum of the same in the T-wave have been used to determine an alternative computation of the total time of ventricular depolarization and repolarization, which is usually determined with the index QT. We have called it "QT_ω" and it is computed as:

$$QT_\omega \; = \; LAST_{max}(\|\omega_n\|_2)^T - \; FIRST_{max}(\|\omega_n\|_2)^Q \tag{12}$$

This index has the advantage of not depending on the always tricky determination of the end of the T wave. An example of the QT_ω index is shown in Fig. 2 for rabbit # 1. Here, it should be observed in the T-wave the amplification of repolarization dispersion.

The classical QT and T_{PE} indices have also been obtained. We have applied a multilead criterion to determine wave boundaries, where QRS_{on} is the earliest reliable QRS-complex onset at any X, Y or Z signals, and T_{end} is the latest reliable T-wave end in the same, applying the rules in [24]. Regarding T-wave peak (T_{peak}), the median of these values in X, Y and Z signals has been computed.

$$\begin{cases} QT = T_{end} - QRS_{on} \\ T_{PE} = T_{end} - T_{peak} \end{cases} \tag{13}$$

2.4. *Population analysis*

Focusing on the drug-induced spatial heterogeneity, we have used two methods to determine the promising feature subset candidates for dispersion markers: 1) Using a two-sided Wilcoxon signed rank test, we have found the indices with statistically significant changes respect to control value (prior to drug supply); 2) Then, we exploit a machine learning approach to develope the attribute selection. This is an important task for avoiding overfitting [25] given the relationship between the number of experiments and the number of indices previously described. The goal was then to reduce the number of attributes to the two most important. In this case, the strategy was to rank the attributes by combining the results of several known attribute selection algorithms.

Regarding feature selection task, we utilized 7 methods: (a) Correlation-based Feature Subset Selection for Machine Learning [26], (b) Relief Attribute Evaluator [27,28,29], (c) Symmetrical Uncertainty [30],

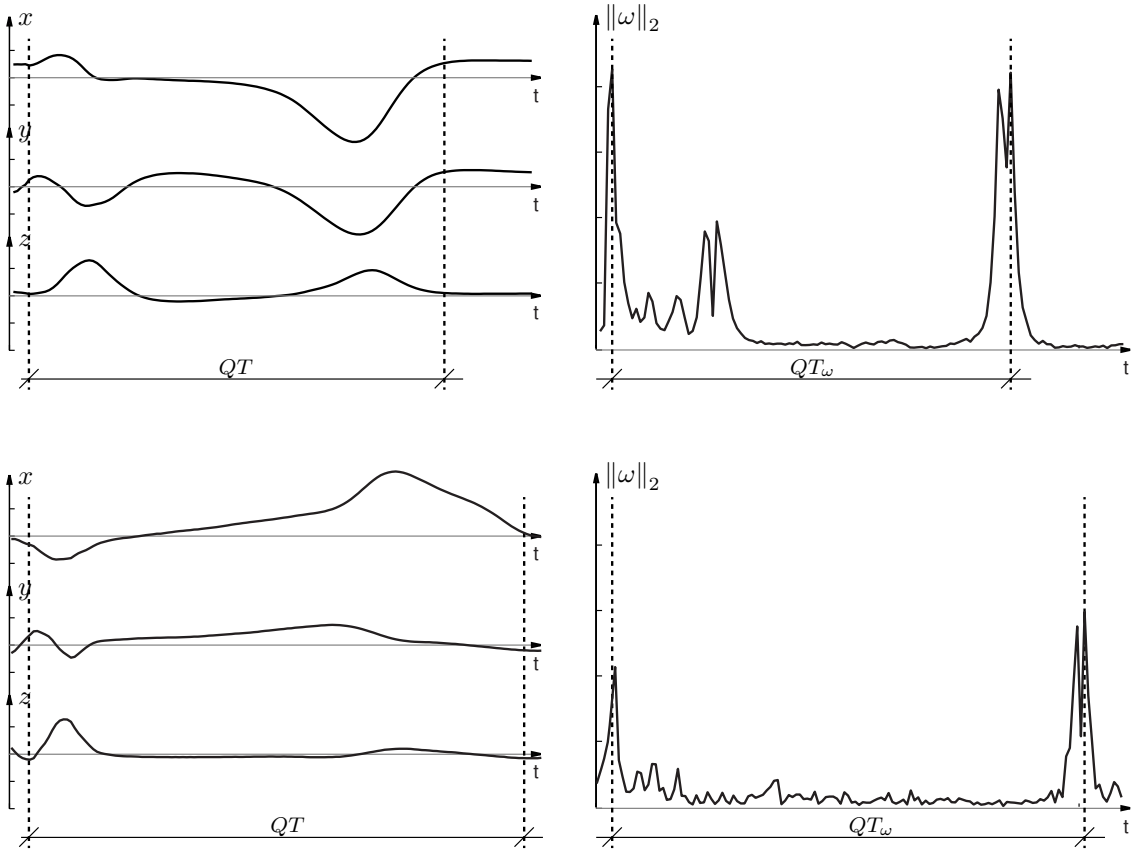

Figure 2. Determination of classical QT interval index (left panel) and the new QT_ω cardiomarker (right panel) in rabbit # 1. In the latter, it can be seen the easiest determination of the end of the repolarization for both cases: Control situation (top panels) and after d-Sotalol supply (bottom panels).

(d) Pearson Correlation [30], (e) One Rule Algorithm [30], (f) Information Gain Algorithm [30], (g) Gain Ratio Evaluator [30]. Each method was assessed in two ways: as a full training set and as a ten fold cross-validation. This resulted in 14 attribute rankings. We counted how many times each attribute was ranked as first, as second, and so on. We assigned linear points from 7 to 1 for each ranking, being 7 for the first and 1 for the last. Finally, we summed all points for each attribute and determined final ranks.

Finally, the best markers are then combined using machine learning techniques. Over the years tenths of methods were developed and in general we cannot define in advance which one is the best for the selected problem. Furthermore, each method requires several parameters to be set, and again this is not known in advance. Therefore we perform experiments to find the best method and the best set of parameters using a mechanism so-called Weka, which treats all the classification algorithms as a single, highly parametric machine learning framework, and uses Bayesian optimization to find a strong instantiation for a given dataset [31]. With this discriminator we show its uncorrelated contribution to the current QT marker. This could provide a promising outcome for applications to the detection of anomalous amplification of dispersion which would be very useful for the definition of standards for proarrhythmic side-effects assessing.

3. Results

Over all the experiments, we evaluated the indices described in Section 2.3. For each case, after 30 minutes of stabilization ten representative heartbeats were extracted. Given the stability of the experiment, the heartbeats did not show significant variability between them, according the method in [32].

Fig. 3 illustrates those parameters with statistical significant variations of ventricular dispersion induced

Index	Placement							Points	**Rank**
	1^{ST}	2^{ND}	3^{RD}	4^{TH}	5^{TH}	6^{TH}	7^{TH}		
$\lambda 21_v^T$	9	0	0	0	1	3	1	73	1
QT_ω	3	1	4	5	1	0	0	70	2
$\lambda 2ET_v^T$	0	9	0	1	3	1	0	69	3
$\lambda 1ET_v^T$	0	1	6	5	1	0	1	59	4
QT	0	1	3	1	7	2	0	48	5
T_{PE}	0	2	1	2	1	8	0	44	6
M_ω^Q	2	0	0	0	0	0	12	26	7

Table 1
Ranking of the 7 best attributes. All the machine learning methods were evaluated as a full training set as well as a 10 fold cross-validation, resulting in 14 attribute ranking.

Rank	Classifier	Accuracy	Mean Absolute Error
1	Logistic Model Tree	95%	0.1739
2	Random Committee	82%	0.1818
3	Adaptive Boosting	78%	0.2299

Table 2
Ranking of the three best classification algorithms using the selected pair of attributes: QT_ω and $\lambda 21_v^T$.

by d-Sotalol supply. Both radius (E) and linear velocity (υ) signals shown a significant rise in their maxima and areas during depolarization phase. In contrast, the angular velocity (ω) in T-wave reported a significant reduction of its area and maximum peak. In this repolarization wave, the area of the radius rises. Also, the location of the maximum peak of the angular velocity shifts to the right under d-Sotalol effects. This clearly implies an increase in the QT_ω index which shows the greatest significance value. As expected, the QT increases in a similar way to the QT_ω. The T_{PE} shows a significant population increase but three cases show reductions. Finally, the ratio of the linear velocity signal eigenvalues in the T-wave shows an increase in the roundness of the velocity loop.

3.1. *Key features and classification*

According to previous Section 2.4, key features were extracted by ranking points. In Table 1, we show all the summed points for each attribute and the final ranks. Then, we applied the clasiffication mechanism to investigate the best pair (QT_ω , $\lambda 21_v^T$) obtained both in feature selection (Table 1) as in statistical significance analysis (Figure 3). All the features were evaluated on the classification algorithms as mentioned above in Section 2.4, resulting the best classifiers in Table 2.

The best classifier for this pair was Logistic Model Tree. Logistic Model Tree is a classification model with an associated supervised training algorithm that combines logistic regression and decision tree learning [33]. For solving classification tasks in statistics, the analogue to linear regression is linear logistic regression, so this method builds classification trees with linear logistic regression functions at the leaves instead of class labels. In our case the the generated tree has only one leaf with symmetric regression functions ρ.

$$\rho = -6.09 + QT_\omega * 0.05 + \lambda 21_v^T * 4.73 \tag{14}$$

This hybrid model produces better predictions and leads to better insights than either model alone. Using this method, it was possible to correctly separate 21 out of 22 experiments (accuracy of 95%), providing the highest pair of sensitivity/specificity (100%/91%) with a likelihood ratio of 11. The same methodology was used by combining two of the best indices of the state-of-art, QT and T_{PE}, throwing a lower accuracy of 86%.

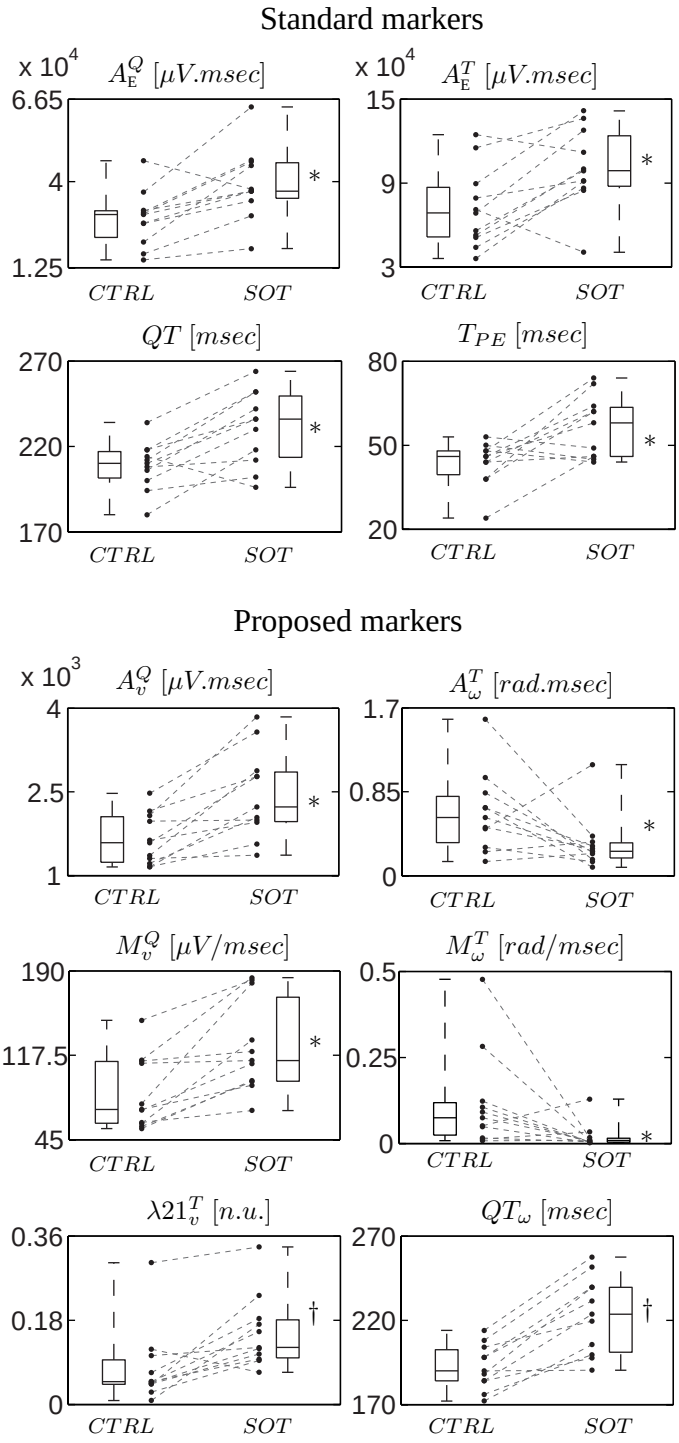

Figure 3. Box and whisker diagrams for significant indices in both control (CTRL) and d-Sotalol (SOT) signals. Individual points are also shown. $*$ p<0.05 and † p<0.01.

4. Discussion

In this work a novel approach of assesing the dynamic features of cardiac vector is proposed by means of an In-Vitro rabbit heart experiment. Changes in heterogeneity are induced by the supply of d-Sotalol, a drug

well-known to have proarrhythmic side effects [34]. The heart was retrogradely perfused through the aorta with Tyrode solution. Firstly, 30 minutes of perfusion with drug-free solution was made. Secondly, d-Sotalol ($60\mu M$) was added to the buffer solution to induce an increase in the dispersion of cardiac repolarization. This model is not the case of oral administration in humans, in which the drug could be distributed in a number of tissues and only a fraction could be absorbed. However, Sotalol has a high level of bioavailability in humans, $F_{abs} > 95\%$ [35]. Although significant beta-blocking effects occur at low values of maximum concentration ($C_{MAX} > 800ng/ml$), Class III effects require higher values. C_{MAX} therapeutic range spans from $1,000$ to $10,000ng/ml$, approximately equivalent to $4\mu M$ - $37\mu M$. Sotalol is not bound to plasma proteins, so the free fraction represents more than 96% in young people, and 95% in elderly [19,20].

In contrast, the concentration used in In-vitro studies usually covers a wide range: $1\mu M$ to $500\mu M$ [17,16,36]. These types of studies seek to observe the increase in heterogeneity or to assess the features of the malignant arrhythmia Torsade de Pointes (TdP). Also, high toxicity has been observed with values greater than $100\mu M$. As the objective of this work was to define spatial dispersion biomarkers, we have used a value greater than twice the maximum concentration used in the clinic, where the effects of changes in heterogeneity become clearly noticeable. Also, the range of values with high incidence of TdP has been avoided. Although future researchs are required to assess the dose dependency of the model, previous works have not observed significant alterations in proarrhythmia variables under the application of different doses close to the maximum effective free therapeutic plasma concentration [37].

On the other hand, the XYZ signal is reconstructed from a mapping set of 30 equally spaced electrodes and its dynamics is studied from the perspective of the state-of-the-art indices and the novel velocity cardiomarkers. The attribute selection techniques shown high consistency with the statistical results. The best attributes which reached the highest rank were QT_ω and $\lambda 21_v^T$. Through different classification algorithms, this pair was able to correctly separate 21 out of 22 experiments.

Regarding the linear velocity, the changes are significant because they are strongly related to the nonuniformity of the conduction velocity and excitability in all the phases of the action potential. It can be noted an amplification of depolarization heterogeneity by the increase of M_v^Q. Also, the increases in the roundness $\lambda 21_v^T$ shows an amplification of repolarization heterogeneity. This implies a significant rise in the dispersion in the whole velocity signal. The abnormalities in linear velocities of the QRS complex and T-wave loops have previously been associated with cardiac risk [13,38].

We have observed that the maximum of the angular velocity of repolarization ω_M^T, turns up towards the end of the T-wave. Its study is relevant since it quantifies the speed of the turns of the cardiac electrical vector in the presence of alterations of the conduction paths [14]. It has been demonstrated that beyond the alterations that arise from damages or anatomical occlusions, the global conduction paths could change due to the modification of the electrophysiological properties [15] such as the alteration of permeability in potassium channels. This increases the likelihood of reentry, increasing the risk of the appearance of malignant arrhythmias. We have observed in Fig. 3 a significant reduction of the maximum M_ω^T and a shift to the right. Clearly this fact influences the significant increase of the QT_ω index, which represents the total duration of the process of ventricular depolarization and repolarization. Given the high significance value observed and its high correlation with QT, it is a significant contribution to the state-of-art as a low uncertainty measure of the prolongation of ventricular activity duration (See Fig. 2). It should be noted that in this model the heart rate is stable due to the pacemaker. Therefore, there is no need to correct the QT. In future human studies, the Bazett formula should be used.

Concerning the observed changes in the QT index, as expected, under the drug effects the duration of the interval is increased accompanied by a rise in T_{PE}. However, the latter index, usually associated to transmural repolarization, presents reductions in 3 cases ($\sim 28\%$); this may indicate that part of the alterations in ventricular heterogeneity occurs in the depolarization phase (QRS complex) or in the first half of the T-wave, during a process mainly dominated by base-apex repolarization. The origin of the temporal dispersion alterations observed in the QT is a long-discussed issue that has not yet been resolved [39,40,41]. Even so, the QT is the index currently used in the drug regulations [1,2].

According to the results observed in Fig. 3, as a consequence of d-Sotalol supply, the absolute areas of the T-wave and the QRS-complex are significantly increased. In this sense, the prolongation of the action potentials would increase the instantaneous magnitudes of the XYZ signal. Our results agree with those

previously found in [32,42].

Finally, the model proposed here would, in essence, allow future screening of many others drugs. However, more research is needed to assess the reproducibility of the method. For the characterization of the model, we have put the initial focus on Sotalol, a Class III drug, which is one of the high-risk compounds included in the CiPA table [11]. This experiment was useful for our objective given that Sotalol modifies the IKr, that is to say, produce an impaired repolarization process. In other words, it induces repolarization instability -heterogeneity augmented- and reduces repolarization reserve. All these factors are potential triggers for arrhythmias. Moreover, In-vitro proarrhythmic studies are being used with greater regularity in the drug study process [17,43,16,36]. Some of the studies of other high-risk drugs, such as Bepidril, Dofetilide and Ibutilide, have shown valuable results for heterogeneity assessment in isolated heart models [44,45,46].

On the other hand, we have previously shown the robustness of the quaternion computation to define risk biomarkers [14]. In this sense, one of the causes for the low specificity of the current ICH S7B/E14 approach could be the difficulty in determining the end of the T-wave, necessary for the automatic computation of the QTc [6]. Our approach is not only independent of wave beginnings and ends, but is more robust in the propagation of numerical uncertainties [23]. Proper development of further studies should achieve promising results regarding quantification of drug-induced increased dispersion.

5. Study limitations

Our original contribution is to present alternative dispersion markers computed from dynamics features that can avoid the need to accurately determine fiducial points, increasing their performance. Although these markers could be very useful in non-invasive cardiotoxicity studies, spatial electrocardiographic signals are obtained from an artificial thorax for In-vitro hearts. Further studies are required to know if we can extrapolate these markers to vectorcardiogram signals.

On the other hand, by combining our two best velocity markers with the standards QT and T_{PE} in a single classifier, we have reached the best performance (100%). However, in this work we consider only pair combinations of potential features taking into account of the 22 total available experiments (up to 2 features: 10%). In the future, with a greater number of recordings, it can be evaluated the usefulness of this combination. It is expected that, beyond the current questions to T_{PE} and QT, their integration with verlocity markers will provide a better description of the spatial dispersion amplification.

Furthermore, many other drugs affect multiple ion channels during cardiac repolarization and they also prolong QT interval or have proarrhythmic side effects [10]. More research is needed so that the relationship of the dynamic features of the cardiac vector and its link to the amplification of drug-induced dispersion can be accounted for thoroughly. As mentioned above, we have used a Sotalol dosage based on the experimental In-vitro rabbit heart model [16,17]; however, the future experiments should be conducted considering different concentrations of each drug given that incresing drug dosage could alter ventricular heterogeneity [47,48]. As well, an accuratelly assess of the influence of both reversible and irreversible inhibition mechanisms on ventricular dispersion would improve our findings. On this basis and future work it can be provided crucial information for the development of safe drug therapies.

6. Conclusions

By means of an experimental procedure, we have shown several dynamic features, some of whom could be very useful for the quantification of amplification of ventricular dispersion, which is associated with proarrhythmic risk. In particular, we have been able to find some characteristics that allow the separation of the control population from the one that received d-Sotalol supply. Additionally, through angular velocity signals of electrical cardiac vector we have exposed a novel technic to measure with high accuracy the QT interval, current index used for the international drug regulation. Successful integration of this ideas with current studies may enable future applications in torsadogenic toxicity studies.

Conflicts of interest

The authors declare that there are no conflicts of interest.

Acknowledgments

This work was supported by CONICET, under project PIP #112-20130100552CO, Argentina. Also, the authors acknowledge the financial support from the Slovenian Research Agency (research core funding No. P2-0098).

References

[1] International Council on Harmonization, S7B the non-clinical evaluation of the potential for delayed ventricular repolarization (QT interval prolongation) by human pharmaceuticals, https://database.ich.org/sites/default/files/S7B_Guideline.pdf (2005).
[2] International Council on Harmonization, E14 the clinical evaluation of QT/QTC interval prolongation and proarrhythmic potential for non-antiarrhythmic drugs, https://database.ich.org/sites/default/files/E14_Guideline.pdf (2005).
[3] M. Brockway, A. Fossa, J. Mason, Comparison of two highly automated ECG algorithms for detection of drug-induced cardiac ion channel block, Clin Pharmacol Ther (2017) doi: 10.1002/cpt.934.
[4] D. Rampe, A. Brown, A history of the role of the HERG channel in cardiac risk assessment, J Pharmacol Toxicol Methods 68 (2013) 13–22.
[5] C. Antzelevitch, J. Di Diego, Counterpoint tpeak-tend interval as a marker of arrhythmic risk, Heart Rhythm 16 (6) (2019) 954–955.
[6] M. Malik, H. Huikuri, F. Lombardi, G. Schmidt, R. Verrier, M. Zabel, Is the tpeak-tend interval as a measure of repolarization heterogeneity dead or just seriously wounded?, Heart Rhythm 16 (6) (2019) 952–953.
[7] H. Huikuri, R. Verrier, M. Malik, F. Lombardi, G. Schmidt, , M. Zabel, Our doubts about the usefulness of the tpeak-tend interval, Heart Rhythm 16 (6) (2019) e49.
[8] N. Stockbridge, J. Morganroth, R. Shah, C. Garnett, Dealing with global safety issues: was the response to QT-liability of non-cardiac drugs well coordinated?, Drug safety 36 (2013) 167–182.
[9] A. Camm, Hopes and disappointments with antiarrhythmic drugs, Int J Cardiol 237 (2017) 71–74.
[10] R. Woosley, K. Romero, C. Heise, T. Gallo, J. Tate, R. Woosley, S. Ward, Adverse drug event causality analysis (ADECA): A process for evaluating evidence and assigning drugs to risk categories for sudden death, Drug Saf 40 (6) (2017) 465–474.
[11] T. Colatsky, B. Fermini, G. Gintant, J. Pierson, P. Sager, Y. Sekino, D. Strauss, N. Stockbridge, The comprehensive in vitro proarrhythmia assay (CIPA) initiative - update on progress, J Pharmacol Toxicol Methods 81 (2016) 15–20.
[12] N. Srinivasan, M. Orini, R. Providencia, R. Simon, M. Lowe, O. Segal, A. Chow, R. Schilling, R. Hunter, P. Taggart, P. Lambiase, Differences in the upslope of the precordial body surface ecg t wave reflect right to left dispersion of repolarization in the intact human heart, Heart Rhythm 16 (6) (2019) 943–951.
[13] P. Cruces, P. Arini, A novel method for cardiac vector velocity measurement: Evaluation in myocardial infarction, Biomed Signal Proc and Control 28 (2016) 58–62.
[14] P. Cruces, P. Arini, Quaternion-based study of angular velocity of the cardiac vector during myocardial ischaemia, Int J Cardiol 248 (2017) 57–63.
[15] F. Burton, S. Cobbe, Dispersion of ventricular repolarization and refractory period, Cardiovasc Res 50 (2001) 10–23.
[16] S. Sossalla, N. Wallisch, K. Toischer, C. Sohns, D. Vollmann, J. Seegers, L. Lüthje, L. Maier, M. Zabel, Effects on ranolazine on torsades de pointes tachycardias in a healthy isolated rabbit heart model, Cardiovasc Ther 32 (2014) 170–177.
[17] M. Zabel, S. H. Hohonloser, S. Beherens, R. L. Woosley, M. R. Franz, Differential effects of d-Sotalol, quinidine and amiodarone on dispersion of ventricular repolarization in the isolated rabbit heart, J Cardiovascular Electrophysiol 8 (1997) 1239–1245.
[18] R. Padrini, G. Speranza, G. Nollo, S. Bova, D. Piovan, R. Antolini, M. Ferrari, Adaptation of the QT interval to heart rate changes in isolated perfused guinea pig heart: influence of amiodarone and d-sotalol, Pharmacological Research 10 (5) (1997) 409–416.
[19] I. Reddy, R. Mehvar, Chirality in drug design and development, Marcel Dekker, 2004.
[20] S. Batul, R. Gopinathannair, Intravenous sotalol - reintroducing a forgotten agent to the electrophysiology therapeutic arsenal, J Atrial Fib 9 (5) (2017) 1–5.
[21] J. Spear, E. Moore, Modulation of arrhytmias by isoproterenol in a rabbit heart model of d-Sotalol induced long QT intervals, American J. Physiol 279 (2000) H15–H25.
[22] P. D. Arini, R. A. Quinteiro, E. R. Valverde, G. C. Bertrán, M. O. Biagetti, Evaluation of QT interval dispersion in a multiple electrodes recording system versus 12-lead standard ECG in an in vitro model, Annals of Noninvasive Electrocardiol. 5 (2) (2000) 125–132.
[23] B. Barsky (Ed.), Rethinking Quaternions. Theory and Computation, Morgan & Claypool, California, 2010.
[24] P. Laguna, R. Jané, P. Caminal, Automatic detection of wave boundaries in multilead ECG signals: Validation with the CSE, Comp Biomed Res 27 (1994) 45–60.
[25] C. Jie, L. Jiawei, W. Shulin, Y. Sheng, Feature selection in machine learning: A new perspective, Neurocomp 300 (2018) 70–79.

[26] M. A. Hall, Correlation-based feature subset selection for machine learning, Ph.D. thesis, University of Waikato, Hamilton, New Zealand (1998).
[27] K. Kira, L. A. Rendell, A practical approach to feature selection, in: D. H. Sleeman, P. Edwards (Eds.), Ninth International Workshop on Machine Learning, Morgan Kaufmann, 1992, pp. 249–256.
[28] I. Kononenko, Estimating attributes: Analysis and extensions of relief, in: F. Bergadano, L. D. Raedt (Eds.), European Conference on Machine Learning, Springer, 1994, pp. 171–182.
[29] M. Robnik-Sikonja, I. Kononenko, An adaptation of relief for attribute estimation in regression, in: D. H. Fisher (Ed.), Fourteenth International Conference on Machine Learning, Morgan Kaufmann, 1997, pp. 296–304.
[30] E. Frank, M. Hall, I. Witten, The WEKA Workbench. Online Appendix for Data Mining: Practical Machine Learning Tools and Techniques, Morgan Kaufmann, 2016.
[31] L. Kotthoff, C. Thornton, H. Hoos, F. Hutter, K. Leyton-Brown, Auto-weka 2.0: automatic model selection and hyperparameter optimization in weka, J Machine Learning Res 18 (1) (2017) 826–830.
[32] P. D. Arini, G. C. Bertrán, E. R. Valverde, P. Laguna, T-wave width as an index for quantification of ventricular repolarization dispersion: Evaluation in an isolated rabbit heart model, Biomed Signal Proc and Control 3 (2008) 67–77.
[33] N. Landwehr, M. Hall, E. Frank, Logistic model trees, Machine Learning 59 (2005) 161–205.
[34] A. Farkas, I. Leprán, J. Papp, Proarrhythmic effects of intravenous quinidine, amiodarone, D-sotalol, and almokalant in the anesthetized rabbit model of torsade de pointes, J Cardiovasc Pharmacol 39 (2) (2002) 287–297.
[35] Y. Yang, P. Faustino, D. Volpe, C. Ellison, R. Lyon, L. Yu, Biopharmaceutics classification of selected beta-blockers: solubility and permeability class membership, Mol Pharm 4 (4) (2007) 608–614.
[36] C. Mackin, E. DeWitt, K. Black, X. Tang, B. Polizzotti, S. van den Bosch, M. Alexander, J. Kheir, Intravenous amiodarone and sotalol impair contractility and cardiac output, but procainamide does not: A langendorff study, J Cardiovasc Pharmacol Ther 24 (3) (2019) 1–10.
[37] C. Lawrence, M. Bridgland-Taylor, C. Pollard, T. Hammond, J.-P. Valentin, A rabbit langendorff heart proarrhythmia model: Predictive value for clinical identification of torsades de pointes, British J Pharmacol 149 (2006) 845–860.
[38] R. Warner, N. Hill, I. Rowlandson, S. Mookherjee, H. Smulyan, Importance of the distance and velocity of electrical forces in the diagnosis of inferior wall healed myocardial infarction: A vectorcardiographic study, Am J Cardiol 57 (1986) 725–728.
[39] M. Merri, J. Benhorin, M. Alberti, E. Locati, A. Moss, Electrocardiographic quantitation of ventricular repolarization, Circulation 80 (1989) 1301–1308.
[40] M. Andersen, J. Xue, C. Graff, T. Hardahl, M. Christiansen, E. Toft, J. Kanters, J. Struijk, Repeatability of T-wave morphology measurements. superiority of a principal component analysis-based lead, Journal of Electrocardiology 40 (2007) S81–S87.
[41] P. Cruces, M. Bonomini, M. Teperino, A. Minchole, P. Laguna, P. Arini, Normal ventricular repolarization dispersion range with abrupt heart rate changes, Computing in Cardiology 41 (2014) 377–380.
[42] M. Zabel, S. Portnoy, M. R. Franz, Electrocardiographic indexes of dispersion of ventricular repolarization: An isolated heart validation study, J. Am. Coll. Cardiol. 25 (1995) 746–752.
[43] J. Steidl-Nichols, G. Hanton, J. Leaney, R.-C. Liu, D. Leishman, A. McHarg, R. Wallis, Impact of study design on proarrhythmia prediction in the SCREENIT rabbit isolated heart model, J Pharmacol Toxicol Methods 57 (2008) 9–22.
[44] T. Osaka, I. Kodama, T. J., K. Yamada, Effects of bepridil on ventricular depolarization and repolarization of rabbit isolated hearts with particular reference to its possible proarrhythmic properties, British J Pharmacol 93 (4) (1988) 775–780.
[45] M. Roche, C. Renauleaud, V. Ballet, M. Doubovetzky, J. Gillon, The isolated rabbit heart and purkinje fibers as models for identifying proarrhythmic liability, J Pharmacol Toxicol Methods 61 (3) (2010) 238–250.
[46] A. Almotrefi, I. Bukhari, M. Alhumayyd, Investigation of the antifibrillatory drug interactions between amiodarone and ibutilide in isolated, perfused rabbit hearts, Fund Clin Pharmacol 29 (2015) 553–557.
[47] D. Zipes, J. Jalife, W. Stevenson, Cardiac Electrophysiology. From Cell to Bedside, Elsevier, 2018.
[48] B. Broux, D. De Clercq, A. Decloedt, L. Vera, M. Devreese, R. Gehring, S. Croubels, G. Van Loon, Pharmacokinetics and electrophysiological effects of sotalol hydrochloride in horses, Equine Vet J 50 (3) (2018) 377–383.